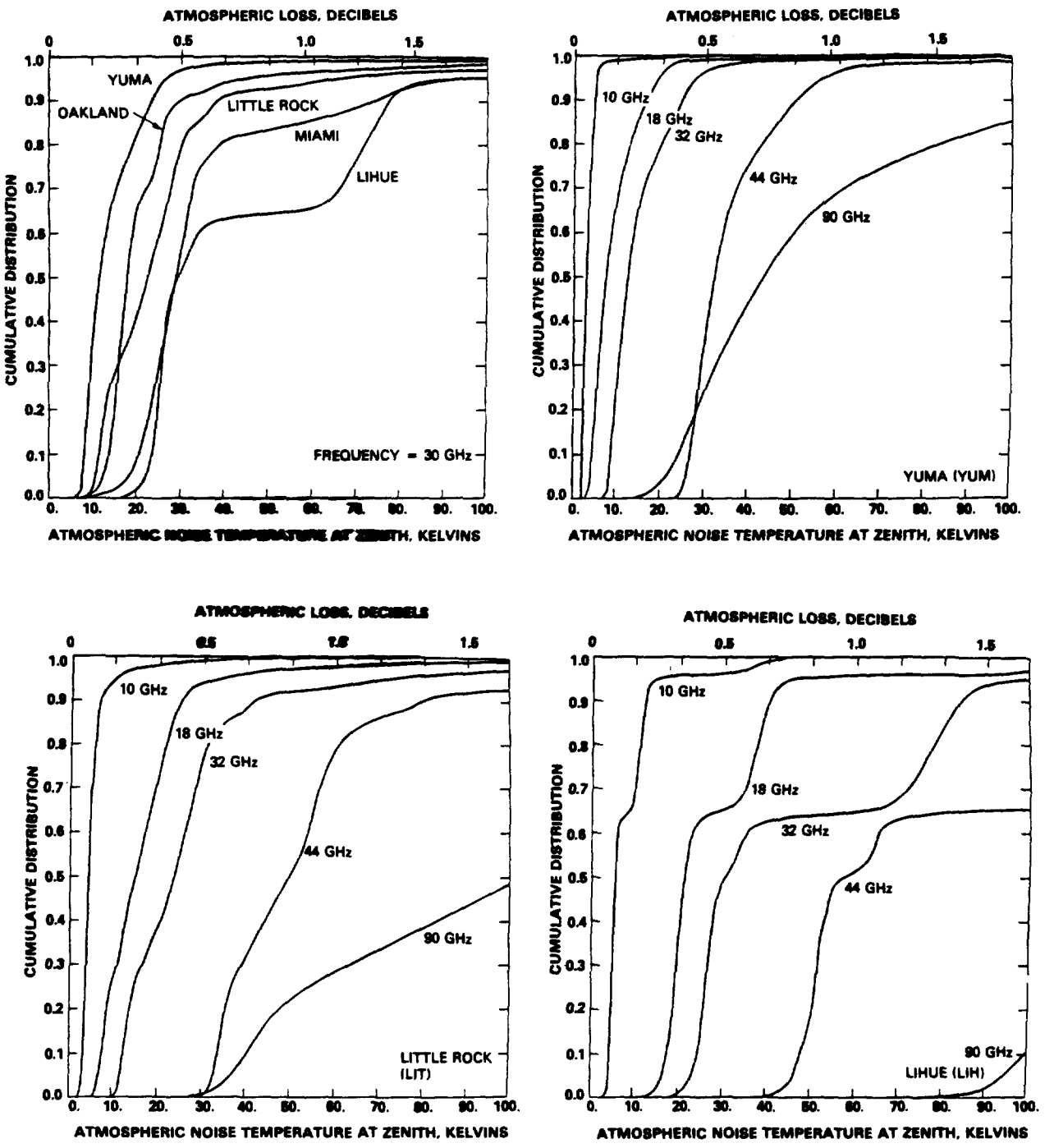

Figure 6.4-3. Examples of Cloud and Gaseous Effects Statustics

Plots of noise temperature and attenuation statistics, both full-year and quarter-year, are available for the 15 regions at 15 frequencies (8.5, 10, 12, 15, 18, 20, 25, 28, 30, 32, 35, 39, 44, 49 and 90 GHz). Interested persons should contact Stephen Slobin, Jet Propulsion Laboratory, Pasadena, CA 91109.

6.4.3 Fog

6.4.3.1 Water Content of Fog. Fog results from the condensation of atmospheric water vapor into water droplets that remain suspended in air. Fog is characterized by optical visibility, which is defined as the distance over which a black target against the sky horizon background can just be discerned by the human eye. The international definition of fog is satisfied when visibility is less than one kilometer (Koester and Kosowsky-1970).

There are two main types of fog, differing in the locale and method of formation. Advection fog is coastal fog that forms when warm, moist air moves over colder water. The liquid water content of advection fog does not normally exceed 0.4 g/m^3. Radiation fog forms inland at night, usually in valleys and low marshes, and along rivers. Radiation fog can have a liquid water content up to 1 g/m^3. Empirical relations have been found (Koester and Kosowsky-1970) between the liquid water content, ρ_ℓ, and the visibility, V(km):

$$\rho_\ell = (18.35\ V)^{-1.43} \text{ for advection fog} \qquad (6.4\text{-}2)$$

$$\rho_\ell = (42.0\ V)^{-1.54} \text{ for radiation fog} \qquad (6.4\text{-}3)$$

6.4.3.2 Attenuation of Fog. The specific attenuation of fog (in dB/km) is estimated using the curves in Figure 6.4-1. The 10°C curve is recommended for the summer, and the 0°C curve should be used for other seasons. Typical liquid water content values for both types of fog vary between about 0.1 and 0.2 g/m^3. The specific attenuation of this, assuming a temperature of 10°, would be about 0.08 to 0.16 dB/km at 35 GHz, or 0.45 to 0.9 dB/km at 95 GHz. (See Figure 6.4-1.) In a typical fog layer 50 m thick, a path at a 30° elevation angle would be in the fog only 100 m, producing less than 0.1 dB of

attenuation at 95 GHz. This suggests that fog attenuation would, in most cases, be negligible.

6.4.3.3 Fog Attenuation Estimation Method. A relatively simple procedure for the estimation of fog attenuation from fog density or fog visibility data has been developed by Altshuler (1984). A regression analysis was performed on a large set of fog attenuation data over a wide range of frequencies (10 to 100 GHz) and temperatures (-8 to 25°C), using tabulated values of indices of refraction. The resulting analysis produced the following expression:

$$a_f = -1.347 + 11.152/f + 0.060f - 0.022T \qquad (6.4\text{-}4)$$

where

a_f is the normalized fog attenuation, in dB/km/g/m^3

f is the frequency in GHz, and

T is the temperature in °C

The total fog attenuation is found by multiplying a_f by the fog density, in g/m^3, and the fog extent, in km. Unfortunately, the fog density is not easily obtainable, and can vary greatly. Fog, however, is often characterized by visibility, which much easier to measure than fog density.

The fog density, M, is empirically related to the visibility, V by;

$$M = (0.024/V)^{1.54} \qquad (6.4\text{-}5)$$

where V is in km, and M is in g/m^3.

The total fog attenuation, A_f(dB), is then available from;

$$A_f(dB) = a_f * M * L_f \qquad (6.4\text{-}4)$$

where L_f is the fog extent, in km.

The standard error of the estimation procedure described above is 0.14 db. The author recommends in a later publication that the procedure should not be used for frequencies below 30 GHz, since the error is comparible in magnitude to the fog attenuation itself (Altshuler-1986).

As an example of an application of the procedure, consider a link at 44 GHz, with a fog visibility of 120 m (0.12 km). The fog density is then

$$M = (0.024/0.12)^{1.54} = 0.0839$$

The normalized fog attenuation, at a temperature of 25°C, will be, from Eq. (6.4-4);

$$a_f = 0.996 \text{ dB/km/g/m}^3$$

The total fog attenuation, assuming a fog extent of 2 km, will then be, from Eq. (6.4-6)

$$A_f \text{ (dB)} = (0.996)(0.0839)(2) = 0.167 \text{ dB}$$

The fog attenuation, as expected, is very low, and is not usually a factor in satellite link system design for frequencies below 100 GHz.

6.4.4 Sand and Dust Attenuation

Sand and dust scatter electromagnetic energy and their effect may be evaluated via Mie scattering. To date simulated measurements have been carried out in the laboratory (Ahmed and Auchterlouis-1976). At 10 GHz and concentrations of sand and dust less than 10^{-5} g/m^3 the measured specific attenuation was less than 0.1 dB/km for sand and 0.4 d8/km for clay. Severe storms have concentrations exceeding these values.

Ghobrial, et al (1978) have calculated a theoretical specific attenuation for sand. Based on the characteristics of particles collected during sandstorms, they conclude that negligible attenuation is suffered by X-band transmissions through sandstorms. This is due to the small particle size compared to the wavelength and the low loss tangent for sand.

Chu (1979) reported that attenuation coefficients from sand particles at microwave frequencies were linearly proportional to frequency, and inversely proportional to optical visibility. The attenuation coefficients for distributions of identical particles were linearly proportional to particle radius. Other theoretical analyses have shown that sand and dust particle attenuation at microwave frequencies tends to be significant at very high particle concentrations (visibilities of less than 20m), or at high moisture contents, or both [Bashir et al. (1980), Ansari and Evans (1982), Goldhirsh (1982)].

Blowing sand and dust storms occur in some regions of the U.S. These are recorded by the Weather Service as part of the Local Climatological Data (LCD) at the 291 stations. Ground stations needing this information should review the data recorded by a nearby LCD recording station.

The vertical extent of these sand storms is unknown, but it seems unlikely that high concentrations would exceed 1 km. The path length is expected to vary between 1/2 and 3 km, generally resulting in a total additional attenuation due to sand of the order of 1 dB or less. No measured satellite beacon link data is available to confirm these results.

6.5 PREDICTION OF SIGNAL FLUCTUATIONS AND LOW-ANGLE FADING ON EARTH-SPACE PATHS

The amplitude, phase, and angle-of-arrival of a microwave signal passing through the troposphere vary due to inhomogeneities in the refractivity (clear air). The effects occur on ime scales shorter

than a minute and on spatial scales shorter than a kilometer. At low elevation angles, the amount of troposphere traversed is significant, and so, below approximately 10 degree elevation angles, low-angle fading must be considered.

6.5.1 Antenna Aperture Effects

The effects of tropospheric turbulences and the antenna can not be totally decoupled because, of course, the measurements and operating systems utilize antennas. The antenna aperture processes the incident wavefront with its spatial and temporal fluctuations into a received signal with only temporal variations.

Wavefront tilt due to inhomogeneities and gradients in the refractivity appear to the antenna as an angle-of-arrival variation. Average elevation angle ray bending is usually 10 times more pronounced than azimuthal ray bending. However, wave tilt fluctuations tend to be randomly distributed in angle relative to the slant path propagation direction, at least when the majority of the path is above the regime of surface effects (surface effects extend upwards several hundred meters).

Fluctuations occurring on spatial scales smaller than the size of the aperture are often referred to as wavefront ripple. This phase incoherence results in an instantaneous gain loss or degradation.

The fluctuations described herein apply to the ground station downlink because its antenna is in close proximity to the turbulent medium. An uplink satellite path will suffer fluctuation gain degradation only due to scattering of energy out of the path. Because of the large distance traversed by the wave since leaving the troposphere, the wave arrives at the satellite antenna as a plane wave (no ripple) and with only minute angle-of-arrival effects. Interference to satellites on the geostationary arc can occur due to the refraction and diffraction of radio relay links oriented toward the satellite.

6.5.2 Amplitude Fluctuations

6.5.2.1 Overview. The phenomena of amplitude and angle-of-arrival fluctuations combine to form received signal amplitude fluctuations. For many cases of propagation one or more of these effects may often be neglected. For example, a receiving system which employs an antenna with a wide beamwidth will not experience angle-of-arrival-induced amplitude fluctuations for most elevation angles. However, such simplification is not always possible. The theory of wave propagation and scattering in random media allows a combination of the turbulence induced effects to be performed in the context of weak fluctuations along a line-of-sight path. The work of Ishimaru (1978), which defines coherent and incoherent field components as a plane wave propagates through a random medium, provides a method of combining amplitude and angle-of-arrival effects into a model of received signal amplitude fluctuation. A model utilizing the concept of incident plane wave decomposition (see Figure 6.6-1) has been proposed by Theobold and Hodge (1978).

6.5.2.2 Variance of Received Signal Amplitude. The assumption of weak turbulence is invoked for a plane wave incident on a region of turbulence, propagating a distance L_t (km) and impinging on a circular aperture of diameter d_a (meters). The antenna is assumed to have a Gaussian pattern function with half-power beamwidth B (degrees). If v_d is the received signal voltage, assuming a square-law first mixer, an expression for signal variance relative to average power is

$$S^2 = 10 \log_{10} \left(\frac{\langle V_d^2 \rangle - \langle V_d \rangle^2}{\langle V_d \rangle^2} \right) \qquad (6.5\text{-}1)$$

$$= 10 \log_{10} \left(\frac{I_c \sigma_1^2 + \dfrac{I_i B^2}{5.55\sigma_2^2 + B^2} - I_i \left(\dfrac{B^2}{2.77\sigma_2^2 + B^2} \right)^2}{I_c + I_i \left(\dfrac{B^2}{2.77\sigma_2^2 + B^2} \right)} \right)$$

where $I_i = 1 - \exp[-L_t/L_0]$

$I_c = (1 - I_i) / (1 + \sigma_1^2)$

σ_1^2 = electric field amplitude variance

σ^2_2 = angle-of-arrival variance (deg^2)

L_t = path length

L_o = a function of density and crosssection of scattering along the path.

Measurements at The Ohio State University of the ATS-6, 20 and 30 GHz beacons as the satellite underwent synchronous orbit transition were used to derive empirical constants for this model. The path length, L_t, was determined as a function of elevation angle, θ, using an effective turbulence height, h_t, of 6 km in the formula

$$L_t = \left[h_t^2 + 2r_e h_t + (r_e \sin\theta)^2 \right]^{1/2} - r_e \sin\theta \qquad (6.5\text{-}2)$$

where r_e = mean earth radius = 6371 km.

The constants were

L_o = 180 km

$\sigma^2_1 = 2.6 \times 10^{-7} f(GHz)^{7/12} L_t(km)^{11/6}$

$\sigma^2_2 = 5.67 \times 10^{-6} L_t(km)^{1.56} d_a (m)^{-1/3}$

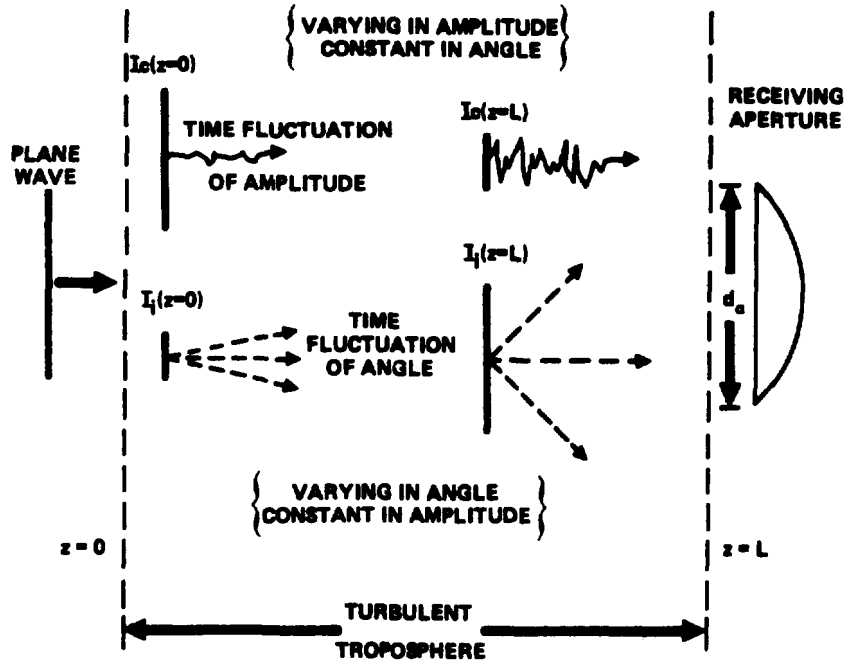

Figure 6.5-1. Decomposition into Coherent and Incoherent Components

A plot of the variance measurement, S^2, expressed in dB, is shown in Figure 6.5-2 for four representative frequencies for a 4.6 m diameter aperture. S^2 is plotted as a function of elevation angle and equivalent path length for a 6 km high region of turbulence.

Figure 6.5-2 represents the average S^2 as derived from the O.S.U. empirical constants. However, since both σ^2_1, and σ^2_2 may be represented in closed form as a function of C^2_n (Tatarski-1961), instantaneous, diurnal, or seasonal values for S^2 may be found from this model given an estimate of the appropriate C^2_n.

6.5.2.2.1 Applicability of the Model. The empirical constants which were found from observed data are applicable for the prediction of average turbulence-induced propagation effects in a temperate climate, during the warmer seasons of the year, and under non-precipitating clear-air conditions. It is necessary to derive local estimates of C^2_n for the model if these conditions are not the same.

6.5.2.2.2 Distribution of Amplitude Variance. It is known that peak-to-peak variations of 30 N-units in the refractive index are expected on a time scale of days and hours (Theobold-1978). Corresponding fluctuations in received signal amplitude variance expressed in dB would be expected to be about 20 dB peak-to-peak for a fluctuation of 30 N-units out of an average of 345. Figure 6.5-3 shows a representative case of average amplitude variance at 30 GHz for a 4.6 m diameter aperture as a function of elevation angle. Curves for plus or minus 10 dB variation in C^2_n about the average are shown for comparison.

A more exact representation of the expected distribution of amplitude variance may be obtained given measured statistics of variance variability about the average. Figures 6.5-4a and b present probability distribution functions of variance differences for 2 and 30 GHz earth-space signals measured over a period of 26 days. The satellite was undergoing transition in elevation from 0.38° to 45° and the mean variance was removed as a function of elevation angle. The 90% confidence limits of 14.6 and 14.7 dB, respectively, are in good agreement with the statistics of expected refractive index variation.

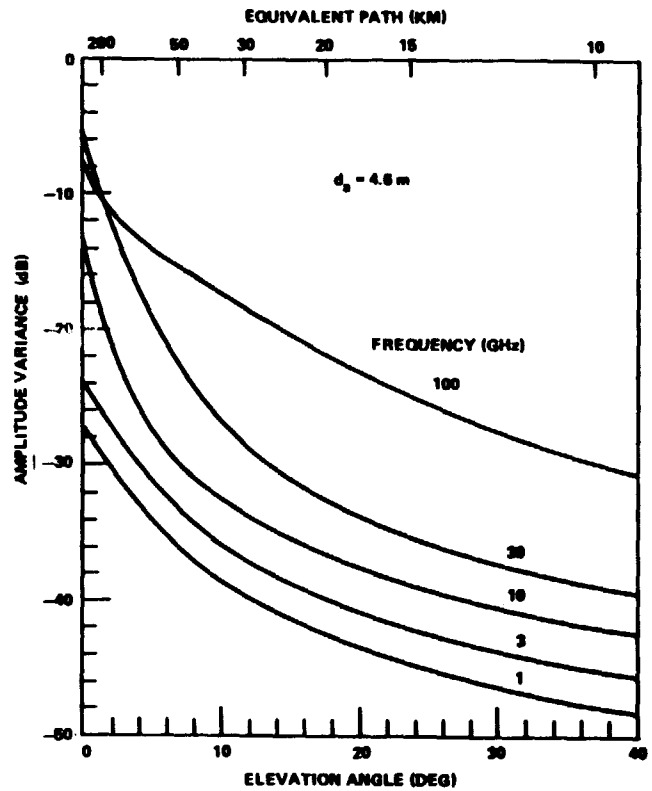

Figure 6.5-2. Amplitude Variance for a 4.6M Diameter Aperture for 1 to 100 GHz

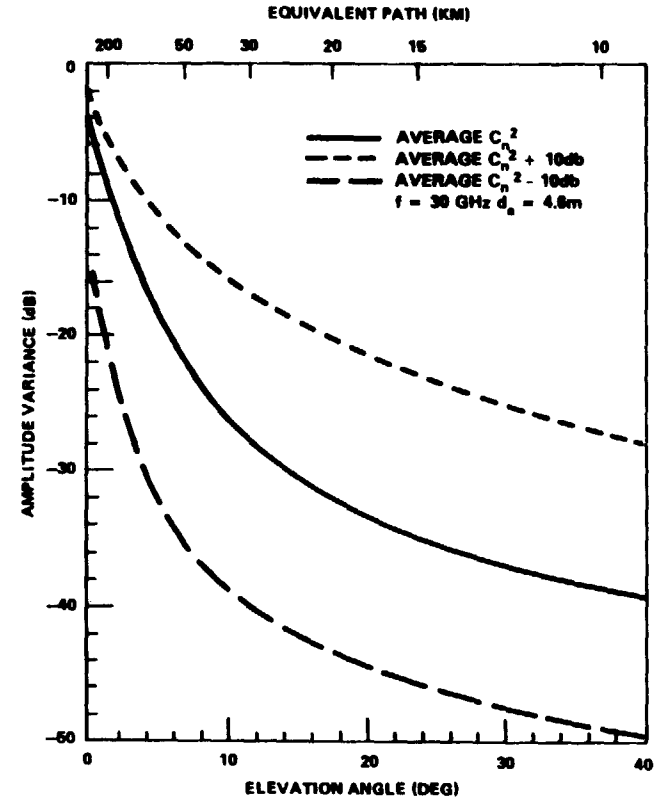

Figure 6.5-3. Effect of 20 dB Peak-to-Peak (30 N-units) Variation of C_n^2 on Amplitude Variance

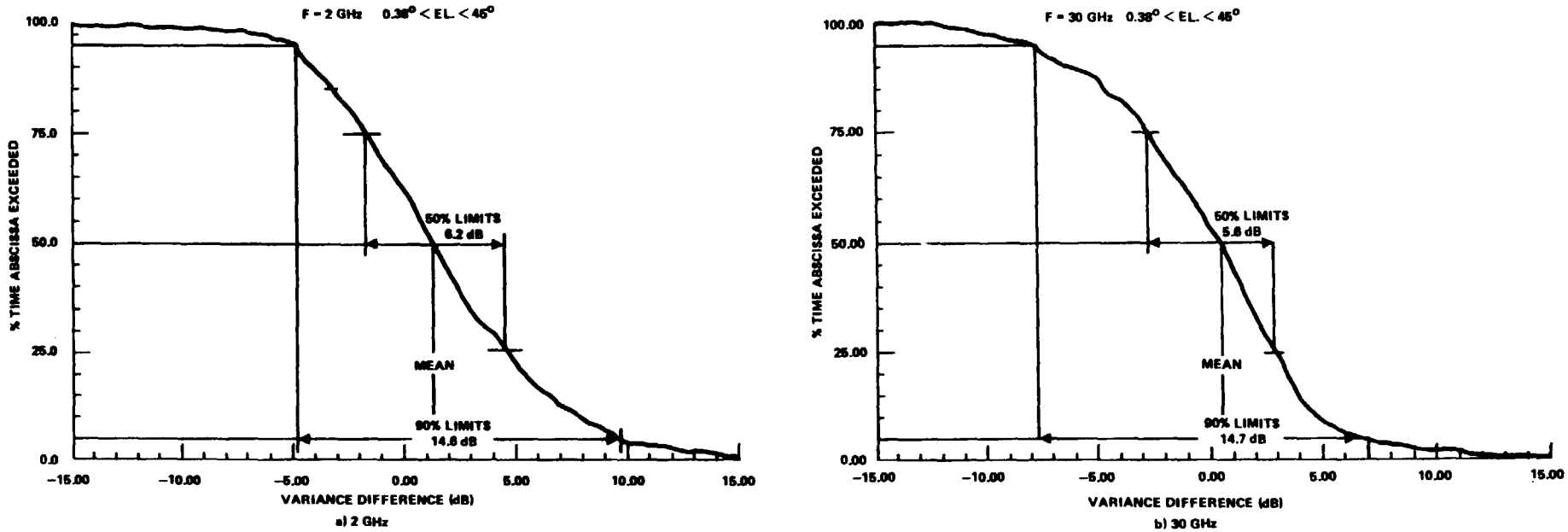

Figure 6.5-4. Distribution of Amplitude Variance from that Predicted from Average Turbulence-Induced Fluctuation Theory

6.5.2.2.3 Power Spectral Density. The formulation of the structure of the power spectral density of turbulence-induced amplitude fluctuations has been derived from classical turbulence theory (Tatarski-1961). The theoretical spectrum of amplitude fluctuations in a medium characterized by a real refractive index is found to roll off as $f_f^{-8/3}$, or -26.6 dB/decade, in fluctuation frequency f_f. This behavior is not a function of operating frequency, as long as the wavelength is small or on the order of the smallest refractive inhomogeneities. Deviation from this slope will occur due to non-stationarity of the scintillation process.

The spectral slope was calculated for time records of 102.4 seconds at 2 and 30 GHz on the ATS-6 CW beacons as the satellites moved in elevation angle from 0.38 to 25 degrees (Baxter and Hodge-1978). Spectral slope was found to be essentially independent of equivalent path length and measured statistics were well centered about the theoretical value of -26 dB/decade. Figures 6.5-5a and b present the probability distribution functions of the 2 and 30 GHz spectral slopes, respectively. Figure 6.5-6 presents the worst-case confidence limits of distribution of spectral slope from an average -26.6 dB/decade, for 50% and 90% of total time. Such an estimate may be used to directly find the expected fading rates and spectral components due to turbulence-induced amplitude scintillation. The data represents clear air statistics over a period of 26 days.

6.5.2.2.4 Estimation of Gain Degradation. The model for received signal amplitude variance has also been used to derive an expression for gain reduction, R, defined by (Theobold and Hodge - 1978)

$$R = 10 \log_{10} \frac{\langle v_d^2 \rangle}{\langle v_d^2 \rangle |_{\text{no angle fluctuations}}} \qquad (6.5\text{-}3)$$

$$R = 10 \log_{10} \frac{I_c + I_i \left[\frac{B^2}{2.77\, \sigma_2^2 + B^2} \right]^2}{I_c + I_i}$$

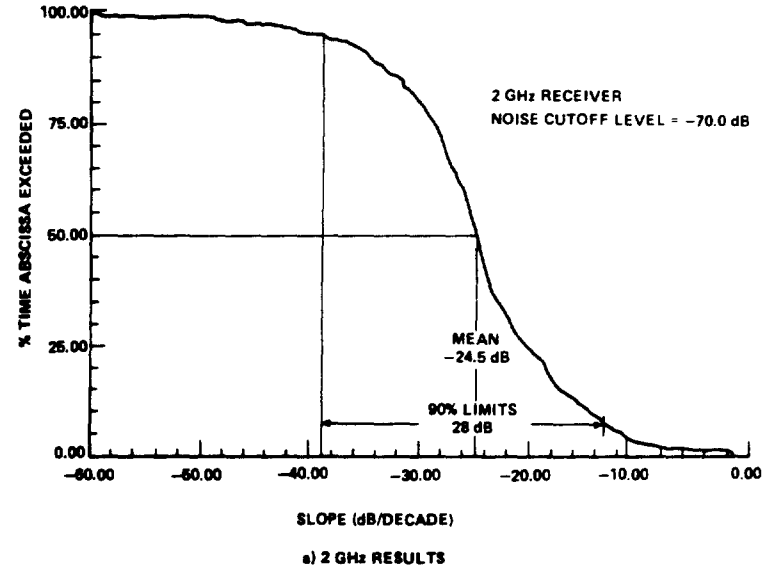

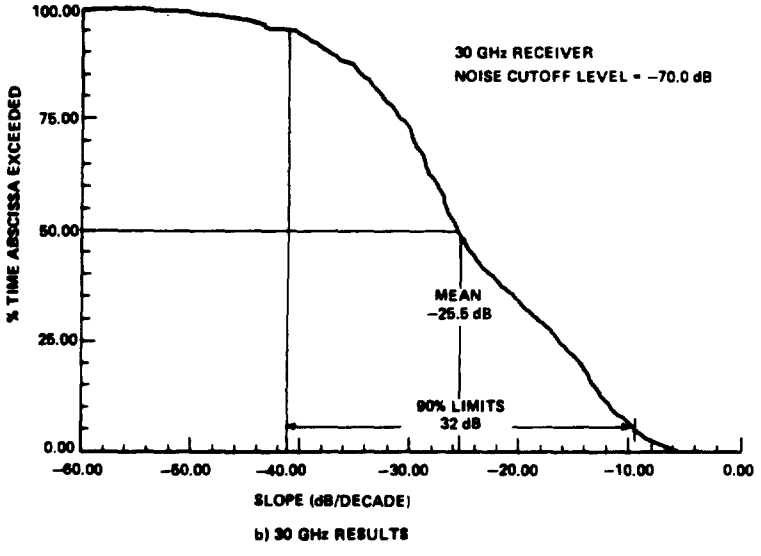

Figure 6.5-5. Probability Density Function of Spectral Slope

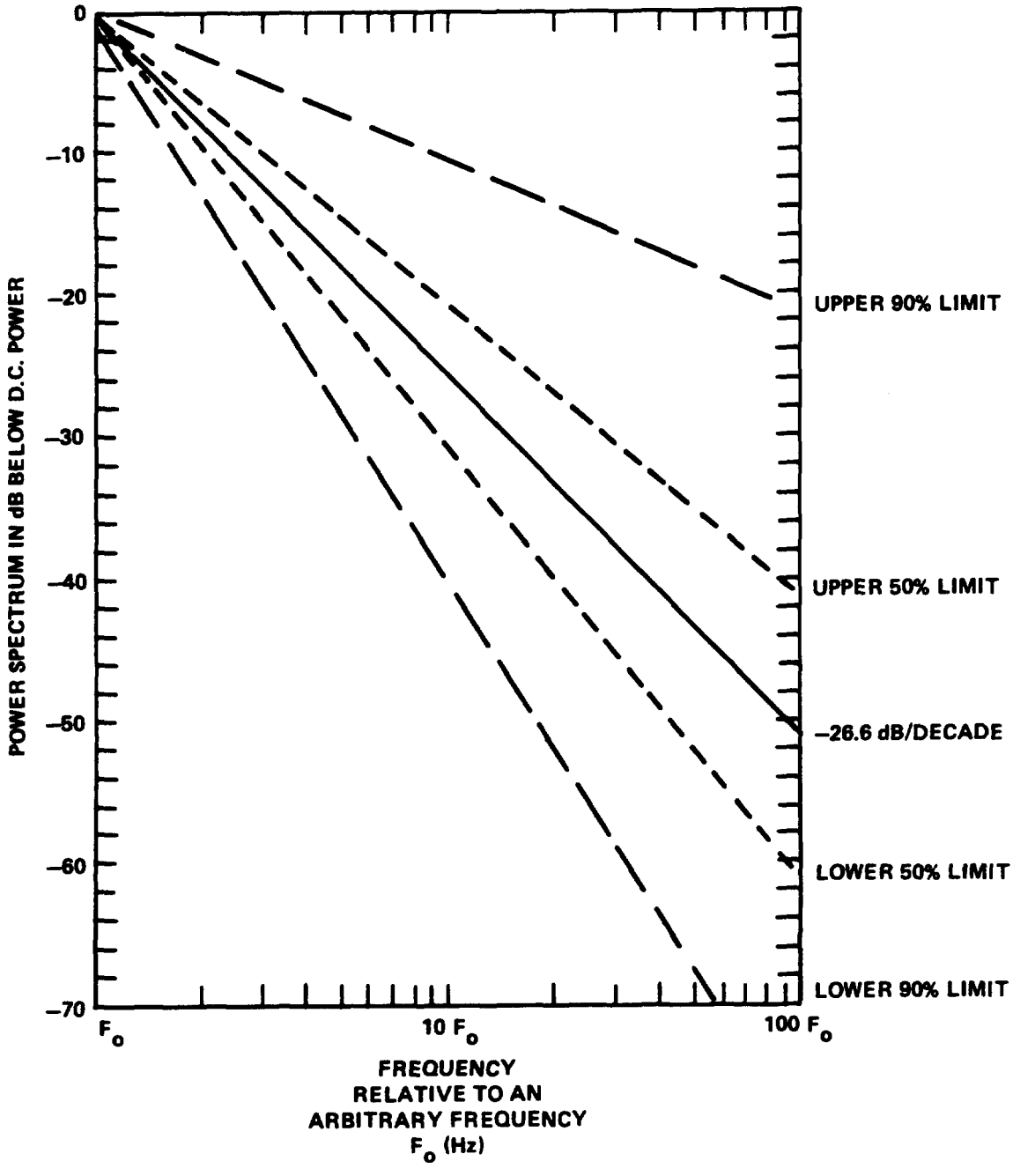

Figure 6.5-6. Confidence Limits of Distribution of Spectral Slope from Average -26dB/Decade

where the constants are the same as those defined for the variance expression, S^2. This value for R may then be combined with atmospheric gas loss in order to obtain an estimate of average received signal level for an earth-space path. Figure 6.5-7 presents an example of predicted signal levels for 2, 7.3 and 30 GHz for antenna beam widths of 1.8°, 0.3°, and 0.15°, respectively. Also included are measured signal levels, relative to zenith, from the ATS-6 2 and 30 GHz (Devasirvatham and Hodge-1977) transmissions and TACSATCOM 7.3 GHz (McCormick and Maynard-1972) beacons as the satellites were moving in elevation angle.

6.5.2.3 Low Angle Scintillations/Fading. At low elevations (typically less than 10 degrees) scintillations and fades occur due to refractive effects and multipath effects in the troposphere. In addition for stations utilizing antennas with significant sidelobe levels intercepting the ground, classic multipath is possible and should be considered. However, the effects reported here are generally thought to not include the effects of ground-reflected multipath.

Because no unified theory for low-angle fading exists, the design of future systems must be done by similarity. As more data becomes available and more systems require low elevation angle operation, undoubtedly a low-angle fading theory will be developed.

6.5.2.3.1 Presentation of Selected Experimental Results. Concise summaries of low-angle fading data and long term statistics for a variety of locations is presented in Tables 6.5-1 and 6.5-2, respectively. These results are typical of the magnitude of the effect, however to date no comprehensive model attempts to explain these effects. A typical plot of the signal amplitude variance at 20 and 30 GHz as observed in Columbus, Ohio between 42 and 2 degrees is shown in Figure 6.5-8 (compare with Figure 6.5-2). Because the distribution suggested a cosecant behavior, a minimum mean-square-error curve was fit to the data as noted in Figure 6.5-8.

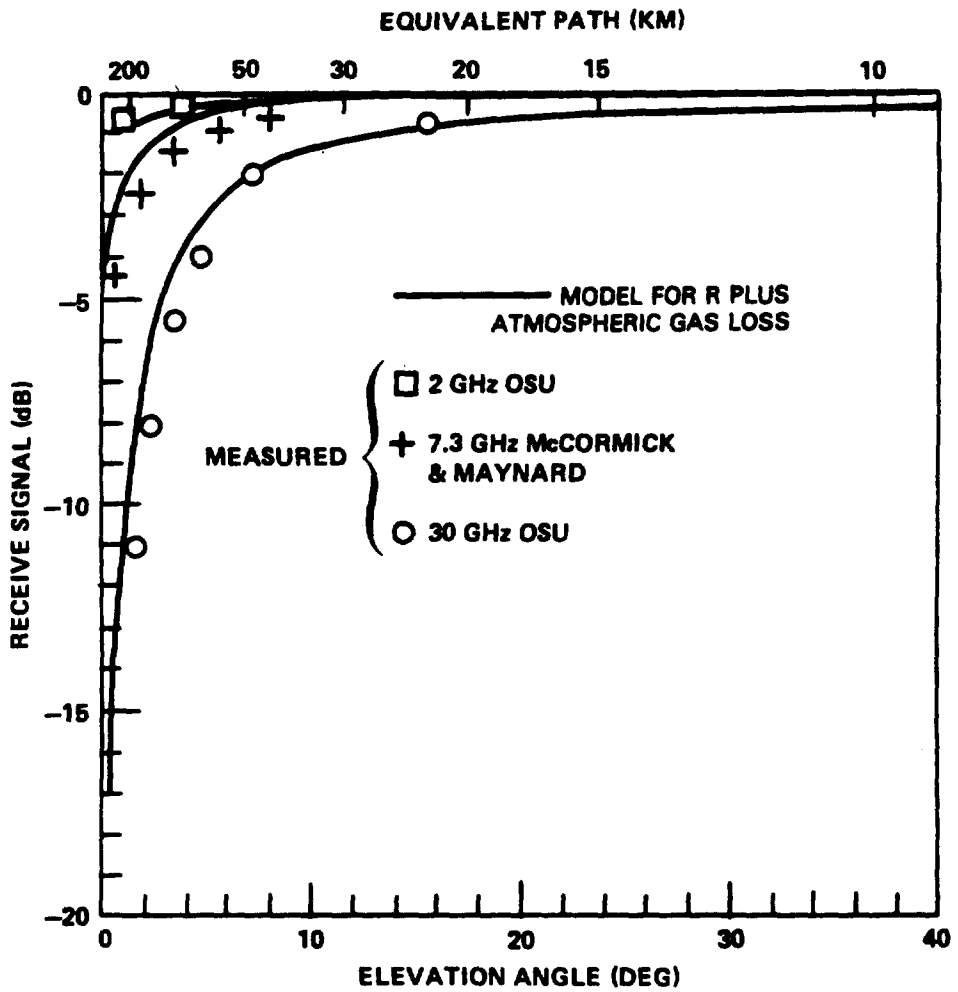

Figure 6.5-7. Predicted and Measured Signal Level as a Function of Elevation Angle

Table 6.5-1. Fading Data Predominantly Due to Scintillation from Satellites at Low Angles of Elevation

[CCIR Report 564-1, 1978]

Location	Satellite	θ (degrees)	Fading data
United Kingdom; Martlesham, Suffolk	ATS-6; 30 GHz	6.5 3.3 2.4	6.5 (dB) (peak-to-peak) 10 (dB) (peak-to-peak) 18 (dB) (peak-to-peak) } Maximum in turbulent windy conditions
		0.3–1.2	Occasional deep fades of 20 dB
United Kingdom; Birmingham	ATS-6; 30 GHz	1–2	Slow enhancements and sudden fades of 20 dB
USA; Virginia [Stutzman *et al*, 1975]	ATS-6; 20 GHz	9 4.7–5.1 4.5	2–3 dB Before and after light rain 2–7 dB Hazy conditions 8–15 dB Partly cloudy conditions
USA; Ohio	ATS-6; 2 and 30 GHz	2.8 0.38	3 dB at 2 GHz 15 dB at 30 GHz 7 dB at 2 GHz 20 dB at 30 GHz } Maximum effect in cumulus clouds
USA; Massachusetts	IDCSP; 7 GHz	10 3	0.03–0.2 dB r.m.s. 10 dB r.m.s. was observed occasionally in summer. Elevation angle fluctuations of up to 0.01° at 3° elevation and 0.002° at 10° elevation (r.m.s values in 5-min period).
Canada; Eureka [Strickland *et al*, 1977]	Anik II; 4 and 6 GHz	1	Data similar at the two frequencies. Fades of 11 and 20 dB predicted for 1% and 0.1 %of worst month.
United Kingdom; Goonhilly [Harris, 1977]	Indian Ocean Satellite, (INTELSAT IV) 4 and 6 GHz	6.5	3 dB (peak-to-peak) exceeded for 0.3% of time on 4 GHz down-link, in a 9-month continuous measurement.
USA; Maryland [Ippolito, 1976]	ATS-6; 20 and 30 GHz	2.5–9	1.5 dB (peak-to-peak) at 9°, increasing to 11 dB at 2.5° at 30 GHz. Values at 20 GHz about 40–70% of those at 30 GHz. Occasional deep fades during light rain.

Table 6.5-2. Statistical Fading Data Predominantly Due to Scintillation and Clear Air Low Elevation Angle Fading

[CCIR Report 564-3, 1986b]

Satellite and frequency	Location of measurements	Antenna diameter (m)	Elevation angle	Peak-to-peak amplitude exceeded for given percentages (dB)					Period of measurement	Reference
				Whole period			Worst month			
				0.1%	0.3%	1%	0.1%	1%		
Intelsat IV-A 3.8 GHz	Oulu, Finland	3	5.4°	3.7	3.2	2.6	4.2	3.2	May 1977-May 1978	[Allnutt, 1985]
Intelsat IV-A 3.9 GHz	Oulu, Finland	3	3.5°	3.7	3.2	2.6	4.5	3.3	July 1979-July 1980	[Allnutt, 1985]
Anik-A 4 and 6 GHz	Eureka, Canada	4.6	1°	–	–	–	20	11		[Strickland *et al.*, 1977]
Intelsat-IV 4 and 6 GHz combined	Goonhilly, United Kingdom (to Bahrain)	30	6.5° (57°)	3.7	3	2.6	4	3	9 months	[Harris, 1977]
Intelsat-IV, 4 and 6 GHz combined	Goonhilly United Kingdom Yamaguchi, Japan	27.5	6.5° 9°	4.6	4.3	3.6	6	5.2		
7 GHz	Ottawa, Canada	9.1	1°	–	–	15	–	–	Summer period	[Webber and McCormick, 1980]
			2-3°	–	–	8	–	–		
			5°	5.5	–	2.8	–	–		
OTS 11.8 GHz	Svalbard Norway	3	3.2°	–	–	–	6.5	3.4	April-December 1979 June-August 1980	[Gutteberg, 1981a]
Intelsat-V 11.45 GHz	Chilbolton, United Kingdom	3	8.9°	4	3.4	2.7	–	–	July-September 1983	[Lo *et al.*, 1984]

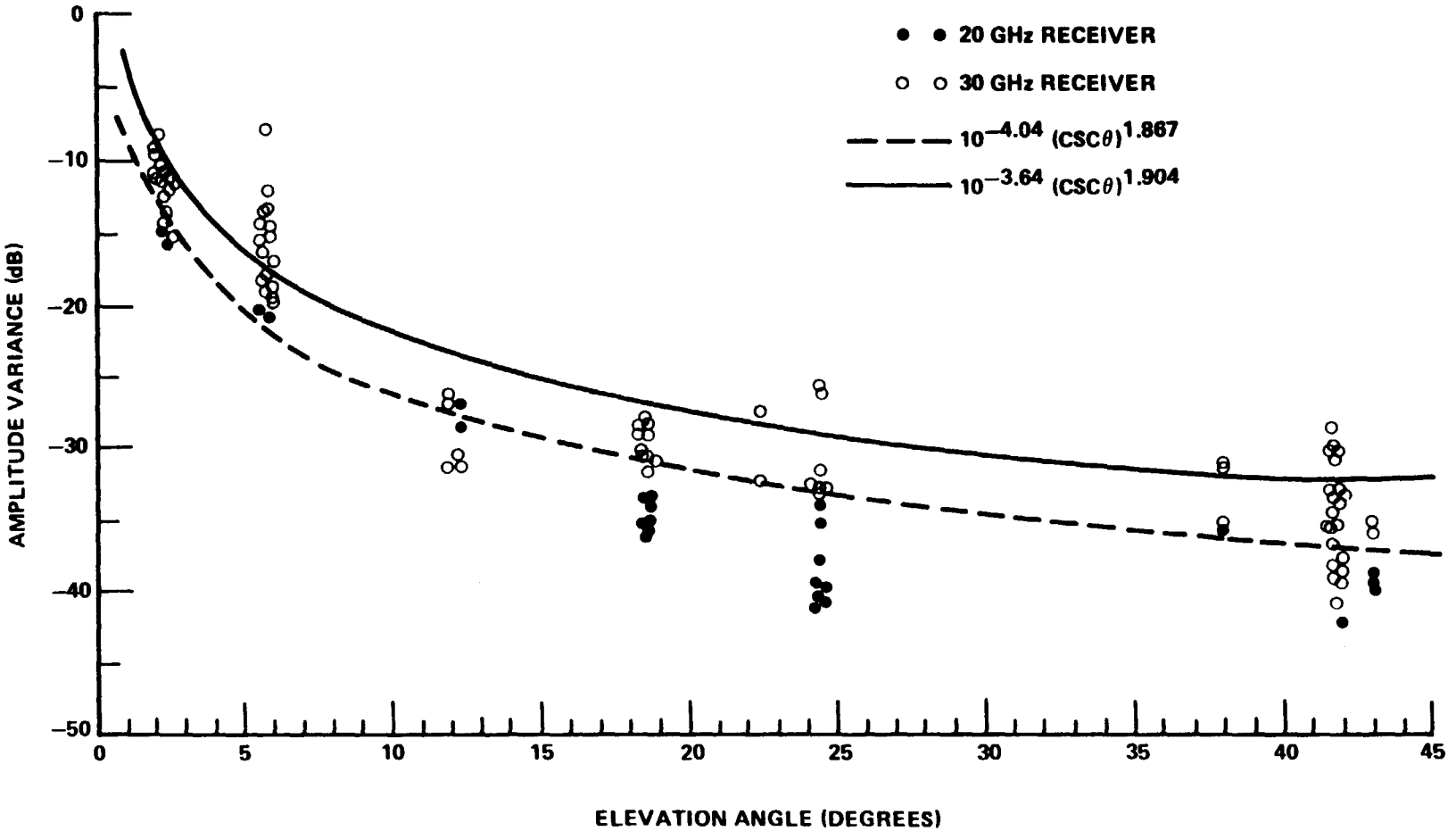

Figure 6.5-8. Measured Amplitude Variance Versus Elevation Angle (Columbus, Ohio)

Experimental measurements of the fade durations at 6 GHz for fades from 0 to 21 dB below the long term median are shown in Figure 6.5.9 (Strickland, et al-1977). These measurements were made at Eureka, Canada during the month of July 1974 when the moisture content (N-value) is above the yearly average. This data is probably typical of continental air mass data. The frequency and elevation angle scaling factors for this data are not thoroughly confirmed, but the Tatarski (1961) model appears to model experimental results (CCIR-1978, Rpt 718). The variance appears to scale proportional to frequency according to the relation:

$$\text{variance} = 42.25\left(\frac{2\pi}{\lambda}\right)^{5/6}\int C_n^2(p)\, p^{5/6}\, dp \qquad (6.5\text{-}4)$$

where p is the distance along the path.

The cumulative distribution for the rate of change of signal amplitude between 0.4 second samples was found to be identical for positive and negative-going signals (Strickland, et al-1977). The measured distribution is given in Figure 6.5-10, but again the frequency and elevation angle scaling factors are unknown.

6.5.3 Phase Variations

Phase variations arise due to the variable delay as the wave passes through a medium with variable refractivity and also due to wavefront ripple introduced by the "lumpy" medium. The former is termed phase delay fluctuations, while the latter effect is called phase scintillations.

6.5.3.1 Estimation of Phase Delay Fluctuations on Earth-Space Paths. An expression for the rms phase fluctuation for a finite circular aperture antenna of diameter d_a,

$$\sigma_\phi = \left(1 - \frac{d_a^2}{4l^2}\right)\left(2L_t l\, \overline{\Delta N^2}\right)^{1/2} \frac{2\pi \times 10^{-6}}{\lambda} \qquad (6.5\text{-}5)$$

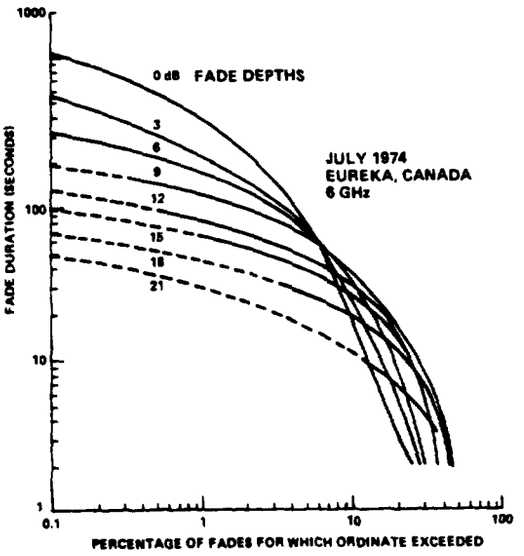

Figure 6.5-9. Cumulative Distributions of Fade Durations at 6 GHz

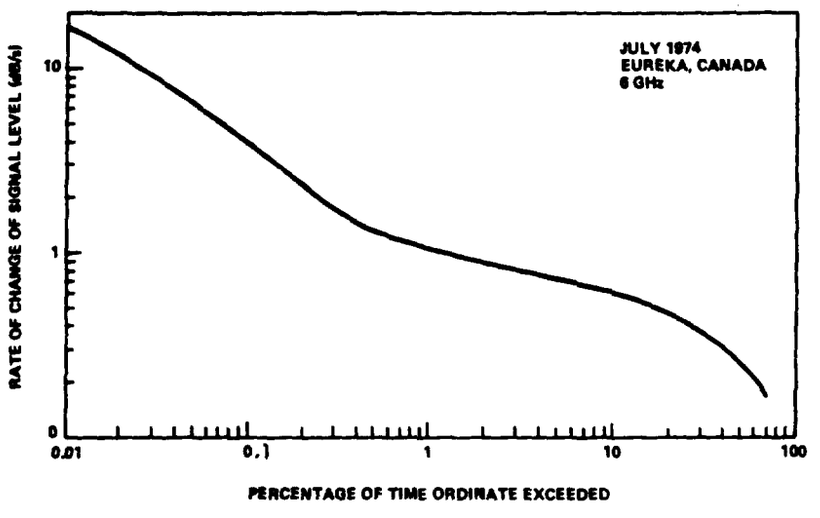

Figure 6.5-10. Cumulative Distribution of Rate of Change of 6 GHz Signal

has been presented by Muchmore and Wheelon (1955). The derivation employs a ray theory approach and assumes an exponental spatial correlation for the turbulence scale. σ_ϕ is in radians, ℓ is the scale length of the turbulent eddy, L_t is the path length through the turbulence, λ is wavelength, and $\overline{\Delta N^2}$ is the mean-square fluctuation in the refractivity N. When using this expression, one should only assume values of ℓ and $\overline{\Delta N^2}$ such that

$$5m \leq \ell \overline{\Delta N^2} \leq 500m. \qquad (6.5\text{-}6)$$

The results of using this relation at the limiting values of $\ell\overline{\Delta N^2}$ for 3 and 10 GHz are presented in Figure 6.5-11. Typical values of ℓ are 60 meters and $\overline{\Delta N^2} = 1/2$. This modeYL indicates that the phase delay fluctuations increase linearly with frequency and become significantly less if the antenna diameter approaches the scale length.

Another technique for estimating these phase delay fluctuations based on the monthly variance of the surface refractivity and estimates of the frequency spectrum of the delay fluctuation have been made by Nusple, et al (1975).

6.5.3.2 Estimate of Phase Ripple Effects on Earth-Space Paths. Accompanying the amplitude scintillations of a plane wave propagating through tropospheric turbulence are transverse phase ripple variations. According to the theory of Tatarski (1961) the mean-square phase variation over a distance transverse to the propagation path is.:

$$D_\phi(\rho_\phi) = K_\phi \, C_{no}^2 (2\pi/\lambda)^2 \, L_T \rho_\phi^{5/3} \qquad (6.5\text{-}7)$$

where λ is wavelength, L_t is the propagation path length through the region of turbulence, and C_{no} is the surface structure constant. The constant K is equal to 2.91 for the exponential C^2_n model (Tatarski-1961) and equal to 4.57 from Ohio data (Theobold and Hodge-1978). This expression may be used to estima- the expected mean-square

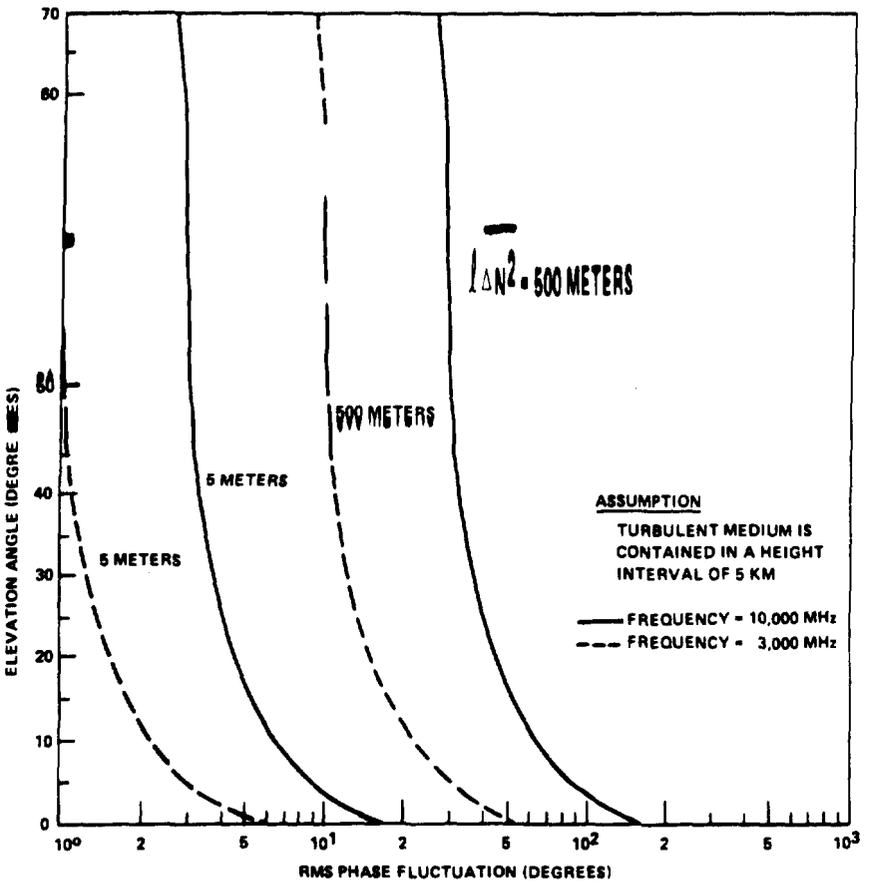

Figure 6.5-11. R.M.S. Phase Fluctuations for an Earth-Space Path

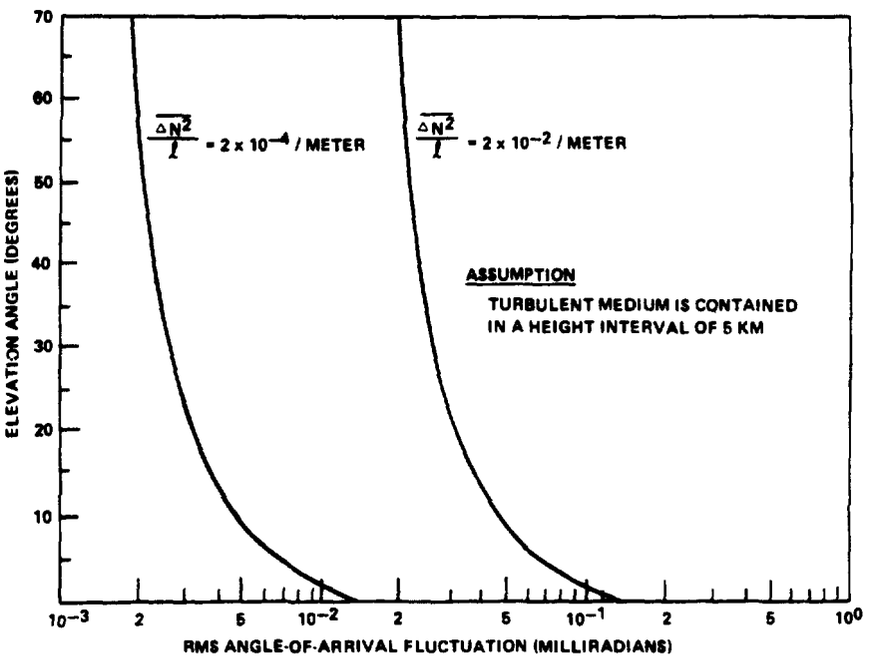

Figure 6.5-12. R.M.S. Angle-of-Arrival Fluctuations for an Earth-Space Path

phase variation between two points separated by a distance ρ_ϕ normal to the direction of propagation, given an estimate of C_{no}.

Clearly, this phase incoherence appears as an apparent antenna gain degradation. Measurements made with a 22 m diameter antenna at 5 degrees elevation angle and 4 and 6 GHz indicate a 0.2 to 0.4 dB degradation (Yokoi, et al-1970). A 7 meter diameter antenna at 5 degrees elevation angle and 15.5 and 31.6 GHz yielded a gain degradation of 0.3 and 0.6 dB, respectively (Yamada and Yokoi-1974). This effect is clearly most pronounced for large antennas, high frequencies and elevation angles below 5 degrees (CCIR 1986b, Rpt. 564-3).

6.5.4 Angle-of-Arrival Variation

The average ray bending (mean deviation from the geometric or vacuum line-of-sight) along a slant path has been estimated by a linear relation to the surface refractivity (Crane-1976a). Estimates of the apparent fluctuations of ray direction or the angle-of-arrival are given below. Because they are assumed to arise solely due to refractive effects the variations are symmetrical about the direction of propagation and the fluctuation frequency is of the order of the time for the turbulence length to pass through the beam.

The Muchmore and Wheelon expression for the rms angle-of-arrival fluctuation in radians is

$$\sigma_\theta = \left[\frac{2\sqrt{\pi}\, L_t\, \overline{\Delta N^2}}{\ell}\right]^{1/2} \times 10^{-6} \qquad (6.5\text{-}8)$$

where all parameters are as previously defined. A Gaussian correlation function for the scale of turbulence was assumed and one should impose the limits

$$2 \times 10^{-4} m^{-1} \leq \overline{\Delta N^2}/\ell \leq 2 \times 10^{-2} m^{-1} \qquad (6.5\text{-}9)$$